Tellus (1993), *45A*, 114–126

Topographic effects in stratified flows resolved by a spectral method

By KJELL ARILD ORVIK and MARTIN MORK, *Geophysical Institute, University of Bergen, Allegaten 70, N-5007 Bergen, Norway*

(Manuscript received 12 December 1991; in final form 28 August 1992)

ABSTRACT

The aim of the paper is to validate a particular model formulation in the study of wind-induced response in a wide, rotating channel with varying bottom topography. The model consists of a continuous stratified upper layer joined to a homogeneous lower layer. For this density profile, standard normal mode solution techniques can be extended to forced models with sloping bottoms in order to separate the vertical dependency. The governing equations are then reduced to a time dependent problem by expanding across channel variations in Fourier series and applying periodic boundary conditions along the channel. An initial-value problem is solved numerically, using an eigenmode solution technique starting from a state of rest, where a constant wind stress is suddenly imposed and then switched off after a certain period of time. The eigenmode solution technique is found to be applicable in the examination of the coupling between vertical modes and the analysis has resulted in a simplified coupling pattern for this specific two layer model. Modified baroclinic eigenmodes are introduced in a superposition of each baroclinic and the barotropic mode, according to the eigenvalue problem. For these modes the interaction amongst baroclinic modes is found to be insignificant while the barotropic eigenmodes are not found to be affected by the stratification. For varying bottom topography these modified baroclinic modes will reflect both stratification and topography. Model simulations show that the flow pattern is dominated by long period barotropic oscillations as topographic Rossby waves. The waves show a dominance in the second lateral mode, and they are less affected by the stratification. The barotropic response to the wind is mirrored in internal displacements and shows long periodic oscillations corresponding to the topographic waves. The use of a bottom Ekman layer has shown that bottom friction mainly influences on long-period barotropic modes. The baroclinic modes are damped by internal friction.

1. Introduction

This study deals with the wind-induced response of a baroclinic ocean with varying bottom topography. Generally, when stratification and topography are both present, the flow field is complicated both physically and from a mathematical point of view. The main approach in this study is therefore to simplify this problem by formulating a two-layer density profile. The two-layer formulation consists of a continuous stratified upper layer joined continuously to a homogeneous lower layer. The study will concentrate on an assessment of the validity of the model and the solution technique applied.

The wind-induced response of a stratified flat bottomed ocean has been studied by many authors. A comprehensive study was performed by Gill and Clarke (1974), who concentrated on wind-induced upwelling. They solved the forced problem by expanding the solution as sums of vertical modes, where the wind forcing was assumed to act as a body force. To some extent they also studied coastally trapped waves when topography and stratification were present. These waves are hybrids between continental shelf waves and internal Kelvin waves.

A study of internal disturbances induced by atmospheric forces over varying topography was performed by Mork (1971) for an abrupt change in depth. Solutions for the forced problem were derived by expansions in vertical modes. The formulation by assuming the eddy viscosity variation with depth proportional to the reciprocal of the static stability (Fjeldstad, 1964) was extended to the forced problem.

For arbitrary stratification and topography, Clarke (1977) showed that wind-forced quasi-geostrophic motions can be described as a sum of modes. He deduced orthogonal eigenfunctions with properties of both topography and stratification. The long wave approximation was crucial in this development of the forced, first-order wave equation. Numerical calculations of these modes have been presented by Wang and Mooers (1976).

Comprehensive discussions of shelf wave dynamics and much of the early theoretical and observational work have been summarized in reviews by Mysak (1980) and Huthnance et al. (1986). Amongst recent, most relevant studies, are Heaps and Jones (1985) and Gordon and Huthnance (1987). Heaps and Jones (1985) studied the dynamic response of a long rectangular stratified sea to wind over a sloping shelf edge, using a three-layered numerical model. Gordon and Huthnance (1987) focused on continental shelf wave response to storms from observations on the Scottish continental shelf by using a barotropic channel model.

The present formulation is to be considered as an alternative approach and makes it feasible to extend standard normal mode separation technique valid for flat bottomed ocean, to a stratified model with varying bottom topography. In order to demonstrate the applicability of the method, a simple geometry of a channel representative for a North Sea section has been chosen. The normal mode procedure will be performed by making use of the Galerkin method in separating the equations vertically and horizontally. Then a quasi-analytic solution technique will be applied to solve the equations as a time dependent problem. This solution technique is suitable for the examination of the coupling and interaction between the baroclinic and barotropic parts of the motion. This assessment will be an important contribution in this study.

The model formulation is close to that of Furnes and Mork (1987) and Furnes (1987). The main differences are in the boundary conditions at the interface between the stratified and homogeneous layers.

2. Model

Consider a two-layer fluid in a wide channel with varying bottom topography, rotating with angular velocity $f/2$. The upper layer is continuously stratified in the vertical and horizontally uniform joined continuously to a homogeneous lower layer. The fluid is incompressible and non-diffusive. The motion will be described relative to a Cartesian coordinate system with the origin in the interface of the undisturbed fluid. As illustrated in Fig. 1, the z-axis is oriented upwards, the y-axis along the channel and the x-axis across the channel. The undisturbed fluid is bounded vertically by the sloping bottom $z=-h$ and the surface $z=H$; horizontally by straight coastlines along the y-axis at $x=0$ and $x=L$. At the surface the fluid is exposed to a wind stress field. Large-scale phenomena relative to the water depth will be considered, so the hydrostatic approximation is justified. The disturbances are assumed to be sufficiently small for the motion to be described by linear theory.

Making use of the Boussinesq approximation, the governing equations may be written as

$$u_t - fv = -p_x + X_z, \qquad (1)$$

$$v_t + fu = -p_y + Y_z, \qquad (2)$$

$$p_z = -\sigma g/\rho_r, \qquad (3)$$

$$\sigma_t + w\rho_{0z} = 0, \qquad (4)$$

$$u_x + v_y + w_z = 0. \qquad (5)$$

The quantities u, v and w are the velocity components in the x, y and z directions respectively, and t is the time. ρ_0 is the density, ρ_r a constant representative density and σ the perturbation density. p is the perturbation pressure divided by ρ_r. The vector $X=(X, Y)$ is the tangential Reynolds stress acting between horizontal planes divided by ρ_r. The acceleration due to gravity g and the Coriolis parameter f are constants, while u, v, w, p, σ are functions of x, y, z and t. The subscripts x, y, z and t signify partial derivatives with respect to these quantities.

Formally, the two layer model formulation results in separate sets of equations for each layer. Appropriate boundary conditions must then be specified at the interface to connect the solutions and at the sea surface, the bottom and the lateral boundaries to complete the equation system.

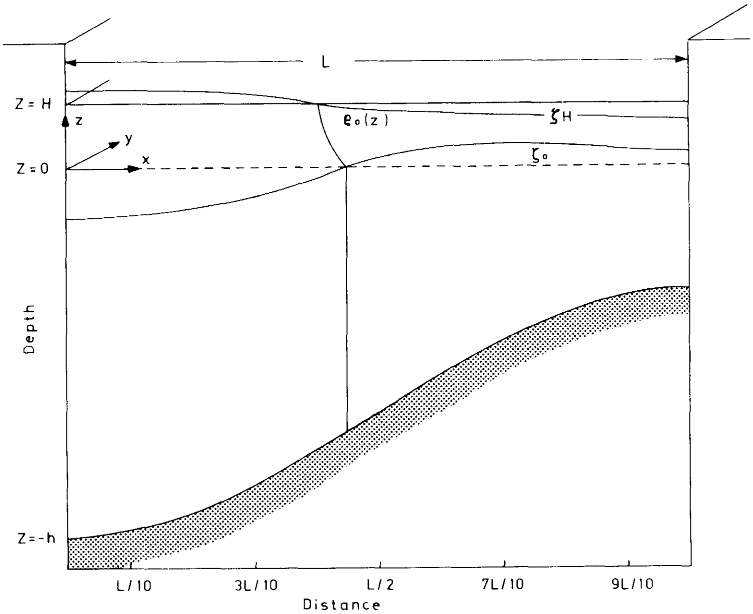

Fig. 1. Sketch of the model with density structure.

2.1. Dynamic boundary conditions

The tangential stress is defined as

$$\boldsymbol{X} = \mu \boldsymbol{v}_z, \tag{6}$$

where $\boldsymbol{v}$ denotes the horizontal velocity $\boldsymbol{v} = (u, v)$. For mathematical convenience the eddy viscosity μ for the upper layer is given by the commonly used formulation (Fjeldstad, 1964)

$$\mu = \alpha g / N^2. \tag{7}$$

The Väisälä-Brunt frequency N is defined as

$$N^2 = -\frac{g}{\rho_r} \rho_{0z}$$

and α is a constant frictional coefficient.

At the surface the stress is defined as

$$\boldsymbol{T} = \mu \boldsymbol{v}_z, \qquad z = H, \tag{8}$$

where $\boldsymbol{T} = (T^x, T^y)$ is a prescribed wind stress.

The surface pressure condition will be

$$p = g\zeta_H, \qquad z = H \tag{9}$$

with no atmospheric pressure forcing. ζ_H denotes the displacement of the free surface.

At the bottom of the upper layer, the interfacial stress is put

$$\boldsymbol{X} = 0, \qquad z = 0, \tag{10}$$

making the Boussinesq approximation. Thus the upper and lower layers are assumed to be sufficiently thick for a frictionless coupling. In accordance with (10), the horizontal velocity in the lower layer is independent of z above bottom friction layer.

At the bottom $z = -h(x, y)$, frictional stress will be included through Ekman boundary layer theory.

2.2. Kinematic boundary conditions

At the surface

$$w = \zeta_{Ht}/\partial t, \qquad z = H. \tag{11}$$

At the interface

$$w = w_0 = \zeta_{0t}/\partial t, \qquad z = 0. \tag{12}$$

ζ_0 denotes the vertical displacement of the interface.

Continuity of density at the level $z = 0$, requires that the tangential velocity components u and v are continuous across the interface.

At the bottom

$$w = -\boldsymbol{v}\cdot\nabla h, \qquad z = -h. \tag{13}$$

At the coastlines

$$u = 0, \qquad x = 0 \quad \text{and } L. \tag{14}$$

2.3. Equations of the lower layer

By applying the appropriate boundary conditions at the level $z = 0$, it follows that u, v and p for the lower layer, can be determined by the governing equations for the motion of the upper layer. Hence by making use of the variables u and v at the level $z = 0$ the vertical velocity w_0 at this level $z = 0$ can be determined by integrating (5) over the lower layer yielding

$$w_0 = -\nabla\cdot\boldsymbol{V}, \tag{15}$$

where vector $\boldsymbol{V} = (U, V)$ denotes the volume transport.

Sub-inertial motion will be emphasized. So bottom frictional effects included through an Ekman boundary layer are justified and the volume transport according to (15) is given as

$$U = u(h - D_e/\pi) - vD_e/\pi, \tag{16}$$

$$V = v(h - D_e/\pi) + uD_e/\pi. \tag{17}$$

A_e is the eddy viscosity for the boundary layer, $D_e = \pi(2A_e/f)^{1/2}$ the Ekman depth and (u, v) the velocity at level $z = 0$.

2.4. Equations of the upper layer

The specific two layer model formulation reduces the problem to solving (1)–(5) for the continuously stratified upper layer with use of the appropriate boundary conditions. Boundary conditions are specified at the level $z = 0$ and the upper layer is then comparable to a stratified channel with a flat bottom. This formulation of the upper layer makes it possible to separate the z-dependency of the dependent variables u, v, p and $w - w_0$ by defining the eddy viscosity μ according to (7). The aim will now be to reduce (1)–(5) to one involving horizontal variations only, by a standard separation technique into normal modes. The solution of (1)–(5) can be found by expanding the dependent variables in terms of a complete set of eigenfunctions as:

$$\boldsymbol{v} = \sum_{n=1}^{\infty} \boldsymbol{v}_n(x, y, t)\cdot\phi_n'(z), \tag{18}$$

$$p = \sum_{n=1}^{\infty} p_n(x, y, t)\cdot\phi_n'(z), \tag{19}$$

$$w = \sum_{n=1}^{\infty} w_n(x, y, t)\cdot\phi_n(z) + w_0, \tag{20}$$

$$\zeta = \sum_{n=1}^{\infty} \zeta_n(x, y, t)\cdot\phi_n(z) + \zeta_0. \tag{21}$$

The eigenfunctions ϕ_n are solutions of an eigenvalue problem

$$\phi_n'' + \frac{N^2(z)}{c_n^2}\phi_n = 0, \qquad 0 < z < H, \tag{22}$$

subject to the boundary conditions

$$\phi_n' - (g/c_n^2)\,\phi_n = 0 \qquad \text{at} \quad z = H, \tag{23}$$

$$\phi_n = 0 \qquad \text{at} \quad z = 0. \tag{24}$$

Here, c_n is a discrete eigenvalue corresponding to a certain eigenfunction ϕ_n. Primes denote derivatives with respect to z.

The eigenfunctions ϕ_n' form an orthogonal set and are normalized by

$$\int_0^H \phi_n'\cdot\phi_m'\,\mathrm{d}z = \begin{matrix}\gamma_n & \text{for} \quad n = m \\ 0 & \text{for} \quad n \neq m.\end{matrix} \tag{25}$$

The wind forcing will be coupled to (1)–(5) through an explicit specification, applying the Galerkin method over the vertical domain. Performing this Galerkin procedure, (1)–(5) are multiplied by arbitrary basis functions ϕ_n or ϕ_n' and integrated over the interval $0 \leqslant z \leqslant H$. Applying the definition (7) of the eddy viscosity μ, integrating the friction terms twice by parts, making use of the eigenvalue problem (22)–(24), the boundary conditions $\mu\boldsymbol{v}_z = \boldsymbol{T}$ for $z = H$ and $\mu\boldsymbol{v}_z = 0$ for $z = 0$ and the condition $\alpha(u, v) \ll (T^x, T^y)$ for $z = H$, the transformed equations for the horizontal will be

$$(\partial/\partial t + \alpha g/c_n^2)\int_0^H u\phi_n'\,\mathrm{d}z - f\int_0^H v\phi_n'\,\mathrm{d}z = -\int_0^H p_x\phi_n'\,\mathrm{d}z + T^x\phi_n'(H), \tag{26}$$

$$(\partial/\partial t + \alpha g/c_n^2)\int_0^H v\phi_n'\,\mathrm{d}z + f\int_0^H u\phi_n'\,\mathrm{d}z = -\int_0^H p_y\phi_n'\,\mathrm{d}z + T^y\phi_n'(H). \tag{27}$$

The transformation of the continuity equation results in

$$-\int_0^H w_z \phi_n' \, \mathrm{d}z = \left(\int_0^H u\phi_n' \, \mathrm{d}z\right)_x + \left(\int_0^H v\phi_n' \, \mathrm{d}z\right)_y. \tag{28}$$

Similarly, the pressure equation is transformed after combining (3) and (4) for elimination of σ. Integrating by parts, making use of the eigenvalue relations (22)–(24) and the boundary conditions at $z = H$, yields

$$\int_0^H p_t \phi_n' \, \mathrm{d}z - c_n^2 \int_0^H w_z \phi_n' \, \mathrm{d}z = w_0 \cdot c_n^2 \phi_n'(0). \tag{29}$$

Substituting the series expansions (18)–(20), making use of the orthogonality property (25), yields the following equation set for each vertical mode

$$(\partial/\partial t + \alpha g/c_n^2)\, u_n - f v_n = -p_{nx} + T^x \phi_n'(H)/\gamma_n, \tag{30}$$

$$(\partial/\partial t + \alpha g/c_n^2)\, v_n + f u_n = -p_{ny} + T^y \phi_n'(H)/\gamma_n, \tag{31}$$

$$-w_n = u_{nx} + v_{ny}, \tag{32}$$

$$p_{nt} - c_n^2 w_n = w_0 \cdot K_n, \tag{33}$$

where $K_n = c_n^2 \phi_n'(0)/\gamma_n$. w_0 is derived from (15) using (16) and (17) and thus depends on all the (u_n, v_n), reflecting the modal coupling.

The eqs. (30)–(33) will be representative for the motion all through the water column. The vertical profile for each mode is to be considered as a vertical mode according to (22)–(24) over the upper layer joined to the lower layer by a barotropic extrapolation.

3. Method of solution

The solution technique which will be aimed is to transform the forced eqs. (30)–(33) in x, y and t into a set of ordinary differential equations in t. Standard methods for solving sets of ordinary differential equations will then be employed. The procedure for reducing the forced equations set will be as follows. A periodic behaviour is assumed in the along-channel direction expressing the y-dependency as products of periodic functions of the form $\exp(i\kappa y)$, where κ is the along-channel wavenumber. The operator $(\partial/\partial y)$ will then be replaced by $i\kappa$.

The separation procedure will be completed by an additional use of the Galerkin method representing the across-channel variations by Fourier series expansions. A half range Fourier series will be applied over the channel $0 \leqslant x \leqslant L$. Both Fourier sine series and Fourier cosine series will form a complete set of basic functions over the interval but they do not form an orthogonal set. The following expansions will be used

$$v_n(x, t) = \sum_{l=1}^{M} v_{nl} \sin(l\pi/L)\, x, \tag{34}$$

$$p_n(x, t) = \sum_{l=0}^{M} p_{nl} \cos(l\pi/L)\, x, \tag{35}$$

$$w_n(x, t) = \sum_{l=0}^{M} w_{nl} \cos(l\pi/L)\, x, \tag{36}$$

$$\zeta_n(x, t) = \sum_{l=0}^{M} \zeta_{nl} \cos(l\pi/L)\, x, \tag{37}$$

where M denotes the number of terms in the series expansion. The bottom profile is assumed to be

$$h = h_0 + \beta \cos(\pi/L)\, x,$$

where h_0 is a constant depth and β a topographic parameter. The Galerkin procedure is performed by multiplying the horizontal equations with the basic functions $\sin(m\pi/L)x$, $m = 1, M$, consecutively for each lateral mode m. The pressure equation is multiplied successively by the basic functions $\cos(m\pi/L)x$, $m = 0, \ldots, M$. The equations are then integrated over the domain $0 \leqslant x \leqslant L$.

Successive application of the Galerkin method reduces (30)–(33) to a set of laterally and vertically coupled ordinary differential equations in t written in a concise and manageable form as

$$\mathrm{d}\boldsymbol{x}/\mathrm{d}t = A\boldsymbol{x} + \boldsymbol{f}(t) \tag{38}$$

where

$$\begin{aligned}x = {} & (p_0, u_1, v_1, p_1, ..., u_M, v_M, p_M)_1,\\ & (p_0, u_1, v_1, p_1, ..., u_M, v_M, p_M)_2,\\ & \vdots\\ & (p_0, u_1, v_1, p_1, ..., u_M, v_M, p_M)_N.\end{aligned} \tag{39}$$

The equation set is then solved by applying a standard eigenmode method expressing the solution as a linear combination of the eigensolutions $\boldsymbol{x}^i = \boldsymbol{v}^i \exp(\lambda_i t)$ of the homogeneous problem. λ_i is an eigenvalue of the matrix A and $\boldsymbol{v}_i$ the corresponding eigenvector.

The eigenfrequencies for the system will be determined by the imaginary parts of the eigenvalues λ_i and the real parts will express the corresponding amplitude functions. The eigenvectors reveal the relative influences of each vertical and lateral mode. For each corresponding eigenfrequency λ_i, the eigenvector will be applicable to reveal coupling and interaction between vertical modes. However, the influence of each eigenmode on the complete flow pattern will not be exhibited. Model simulations have to be performed to reveal the significant eigenmodes.

The model will be run for an initial-value problem, starting from a state of rest. The response of the flow field to a suddenly imposed wind forcing, switched off after a certain period, will be analyzed. The lateral wind stress profile is chosen as

$$\boldsymbol{T} = \boldsymbol{T}_0 \sin(\pi/L)\, x,$$

fitting the boundary condition of no flow through lateral boundaries.

The feature of the time series, with emphasise on the interfacial oscillations ζ_0 and horizontal currents at levels $z = 0$ and H will be discussed. Special consideration will be given to topographic effects and bottom friction.

The following parameter values will be used: $(T_0^x, T_0^y) = (0, 1)\ \mathrm{Nm}^{-2}$, $L = 400$ km, $H = 55$ m, $h = 195$ m and $\beta = 100$ m. α is to be $10^{-7}\ \mathrm{ms}^{-1}$ and $f = 1.26 \cdot 10^{-4}\ \mathrm{s}^{-1}$, corresponding to a latitude of 60° N. The density profile used and the eigenvalue-problem (22)–(24) is solved according to Furnes and Mork (1987). The model is analyzed for wavelengths $2 \cdot 10^2\ \mathrm{km} \leqslant y \leqslant 2 \cdot 10^4$ km. 14 vertical modes and 5 lateral Fourier modes are used in the model simulations.

4. Eigenfunctions

Generally, the model responds in a well-defined set of frequencies. The complete spectrum consists of modified Kelvin waves and an infinite number of modified Poincare modes of increasing order. Additionally, the dispersion curves corresponding to the case of stratification and sloping topography presented in Fig. 2 show evidence of topographic Rossby waves. The eigenvectors reveal that these sub-inertial eigenmodes are prominent mainly in the barotropic mode and less influenced by the stratification. The dispersion curves in Fig. 2 show non-dispersive waves at low wave numbers with increasing frequencies towards a maximum for a certain wavelength corresponding to zero group speed (hereafter be denoted ZGS). For the gravest mode (also denoted first mode), the frequency reaches the maximum for a wavelength of about 700 km with a minimum period of about 87 h. The corresponding values for the longer-period second mode are 250 km and 170 h.

The lateral current profiles for the Rossby waves show oscillatory patterns across channels. Generally, the lateral nth-mode topographic wave has n nodal lines in the across-channel velocity and $n+1$ nodal lines in the along-channel velocity. The lateral profiles shown in Fig. 3 fit well to this property.

For the Poincare waves the sloping bottom does not affect the frequency significantly. There is a modification of the across channel amplitude towards a more antisymmetric oscillatory pattern and displacement of the nodal lines. The barotropic Kelvin waves trapped along the coastlines change character and are modified in an asymmetric pattern. The modifications are manifested through different frequencies for the propagating directions because the phase speed of the Kelvin wave follows the long wave relation and is thus reduced in shallow water. With respect to the lateral amplitude distribution shown in Fig. 3, the exponential Kelvin wave structure is maintained for the along-channel velocity. The deviation from the Kelvin wave type is manifested by a significant velocity component across the channel.

4.1. *Effects of bottom friction*

The influence of internal and bottom friction on the eigenmodes will be analyzed in a gross sense. So the frictional influence on amplitude changes

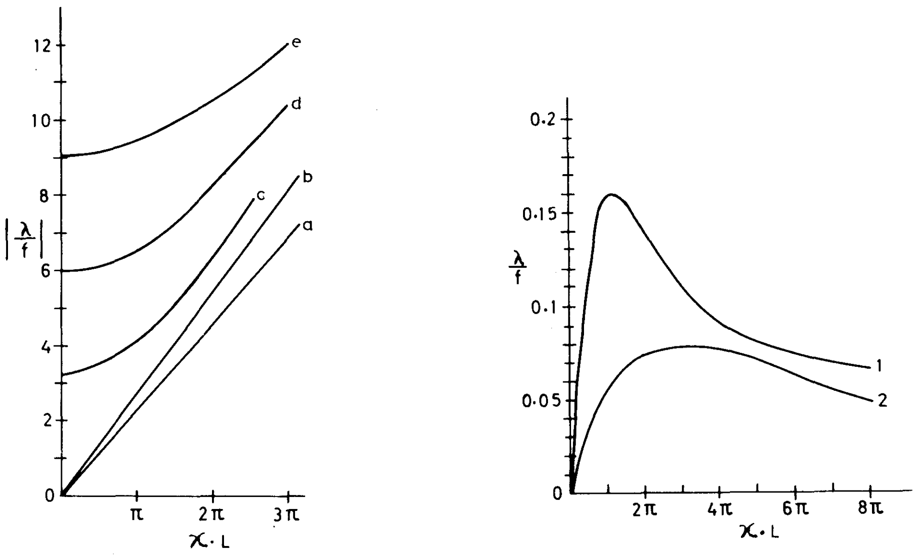

Fig. 2. Calculated eigenvalues for matrix A presented as non-dimensional dispersion curves for waves propagating in y-directions. (a–b): Kelvin waves propagating in opposite directions. (c–e): Three first Poincare wavemodes. (1–2): Two first Rossby wavemodes.

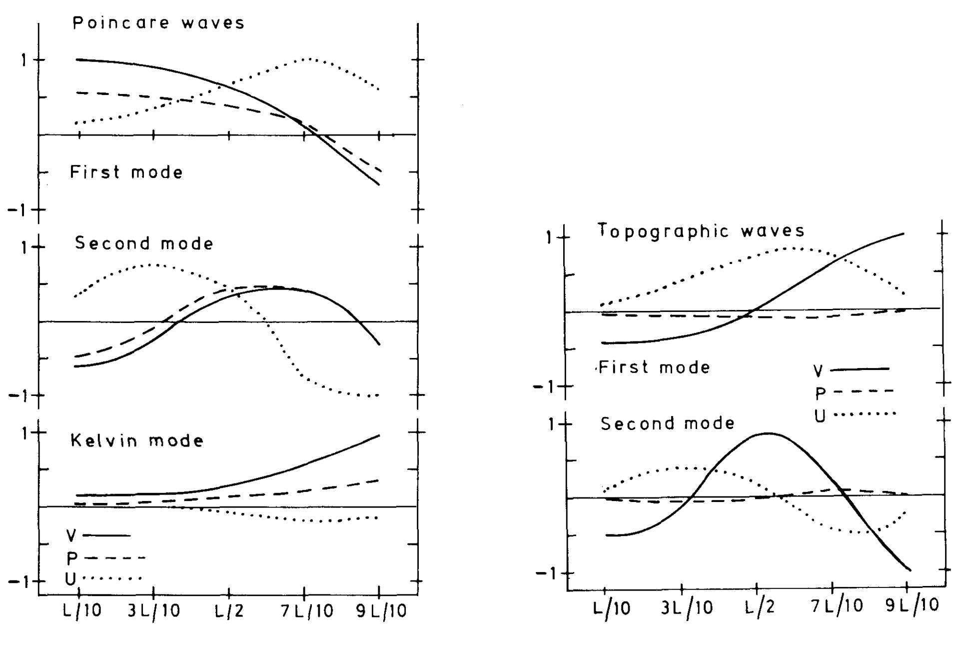

Fig. 3. Lateral amplitude functions determined from the corresponding eigenvectors for the waves in positive y-direction.

Table 1. *The e-folding parameter in hours for selected eigenmodes calculated from the real part of the eigenvalues of matrix A*

	No bottom friction	Bottom friction Ekman depth 5 m	10 m
1st baroclinic wavemode	16.6	16.6	16.6
2nd baroclinic wavemode	4.3	4.3	4.3
1st Rossby wavemode	$6 \cdot 10^3$	300	155
2nd Rossby wavemode	$2 \cdot 10^3$	260	140

and effects as phase speed changes, tilting of co-phase lines and phase lag between current and vertical displacement of the isopycnals are outside the scope of this work.

Apart from the bottom Ekman layer, the calculated eigenvalues in Table 1 fit well to the frictional coefficients $\alpha g/c_n^2$. Hence the barotropic eigenmodes for the topographic waves are less affected by the internal friction and propagate as undamped waves. For the baroclinic eigenmodes, the frictional damping is considerable and the higher wavemodes are the most damped.

Table 1 shows that bottom friction mainly affects the long-period barotropic waves. The damping is strongly dependent on the thickness of the frictional layer. The baroclinic eigenmodes are according to Table 1 unaffected by the bottom friction. Consequently, the damping of the barotropic phenomena is steered by the bottom friction while the baroclinic waves are damped by internal friction. The eigenvalues also reveal that the phase speed properties of the topographic Rossby waves are not significantly affected by the bottom friction.

4.2. Barotropic-baroclinic coupling

Formally for the modes according to (22)–(24), the coupling between mode n and each of the mth modes where $m \neq n$, can be deduced by writing (33) explicitly for modes n and m. Combining the equations, yields

$$p_{nt} - c_n^2 w_n = (K_n/K_m)(p_{mt} - c_m^2 w_m). \tag{40}$$

Because $c_1^2\gamma_1^{-1} \gg c_2^2\gamma_2^{-1} > \cdots > c_N^2\gamma_N^{-1}$ and thus $K_1 \gg K_2 > \cdots > K_N$, it follows that $K_n/K_m < 1$ for $m < n$ and $K_n/K_m > 1$ for $m > n$. So it seems reasonable to anticipate that coupling between the nth mode and the mth mode will be reduced successively as increasing the order of the mth mode. Because $K_1 \gg K_n$, $n = 2, \ldots, N$, the coupling between each baroclinic and the barotropic mode will be of a different character.

The eigenvectors corresponding to the barotropic eigenmodes, exhibit no significant coupling with the baroclinic field. Thus the topographic Rossby wave features are revealed only in the barotropic mode. This result agrees with that of Furnes (1987), who found little influence of varying density fields on the long periodic oscillations. This is presumably due to the fact that stratification lies above the topography (Allen, 1975; Wang, 1975).

The baroclinic eigenmodes were identified from dispersion relations as Poincare waves with frequencies just above f. For each eigenmode, the corresponding eigenvector exhibits a coupling between the specific baroclinic and the barotropic mode (according to (22)–(24)). This simplified coupling pattern of vertical modes can be written as

$$p_{1t} - c_1^2 w_1 = -K_1 \sum_{j=1}^{N} ((U_j)_x + (V_j)_y), \quad j = 1, \ldots, N \tag{41}$$

for the barotropic mode and

$$p_{nt} - c_n^2 w_n = -K_n((U_n)_x + (V_n)_y + (U_1)_x + (V_1)_y) \tag{42}$$

for each baroclinic mode, $n = 2, \ldots, N$.

These simplifications are to be considered hypothetical and have to be verified by running the simplified model and the complete model for similar conditions. The simulations will be performed in Section 5.

Additionally, the baroclinic eigenvectors exhibit an approximately constant relation between the baroclinic and barotropic contribution as

$$u_{e1}/u_{en} \approx h/(H+h), \qquad v_{e1}/v_{en} \approx h/(H+h), \tag{43}$$

where $\boldsymbol{v}_{e1}$ denotes the barotropic and $\boldsymbol{v}_{en}$ the baroclinic part. This interaction can be interpreted as linear superposition of modes, as illustrated for the first baroclinic eigenmode in Fig. 4.

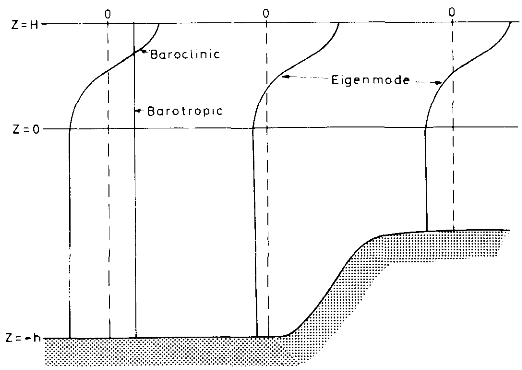

Fig. 4. Sketch to illustrate how the first baroclinic eigenmode is obtained as a superposition of the baroclinic and barotropic contribution.

The relation (43) reveals that the superposition results in eigenmodes with an insignificant volume transport over the depth. Thus, the model responds in baroclinic eigenmodes of the same form as baroclinic modes for stratified flat bottomed oceans.

By assuming $h \gg H$, it follows from (43) that $u_{1e} + u_{ne} \approx 0$ and $v_{1e} + v_{ne} \approx 0$. Thus for a deep lower layer, the response will be manifested in the upper layer with small velocities in the lower layer. For a shallower lower layer where h is of the order of H, the response will extend all through the water column.

Because the eigenvectors exhibit a modal superposition in a fixed relation according to (43), these baroclinic eigenmodes will be functions of both the across-channel coordinate x and the vertical coordinate z, reflecting both stratification and topography. These vertical modes are comparable with the two dimensional modes shown by Clark (1977) in a shelf model.

5. Model simulations

The model response at different wavelengths will be discussed. Starting from the state of rest, the wind stress is imposed and then switched off after 30 h. To resolve short periodic oscillations the model is firstly run for a period of 100 h for 700 km wavelength. The time series are presented in Fig. 5, showing the response for the horizontal velocity components and the interfacial displacement ζ_0. To verify the coupling hypothesis a similar run is performed for the simplified coupling model, presented in Fig. 6. Comparing the results by inspection of the time series, no significant disagreements are revealed confirming the coupling hypothesis.

Then, similar runs are performed for wavelengths of 700 km and 2000 km, presented in Figs. 7 + 8. For these simulations short periodic oscillations are not resolved in the presentations. Finally, simulations are performed with an Ekman layer of thickness 5 m (Fig. 9).

Fig. 5 shows that the initial response to the wind forcing gives rise to inertial oscillations. The oscillations are expressed by sums of Poincare waves and correspond to solutions given for flat bottomed channels (Fennel, 1989).

It is apparent from Fig. 5 that the Ekman pumping produces a direct response in the baroclinic field. This is manifested through the displacement of the interface ζ_0. For the forcing period, a linearly increasing cosine-formed displacement develops. When the wind is switched off, a reversed current pattern develops where inertial oscillations are excited anew. However, sub-inertial oscillations are generated by the cross isobathic flow, and it is apparent from the figure that these oscillations are the dominating contribution to the flow field.

Figs. 7 and 8 reveal a barotropic flow field where the long-period oscillations are identified as free Rossby waves. Fig. 7 shows periodic oscillations reflecting the gravest and second Rossby mode with periods of 87 h and 225 h. A striking feature of the flow pattern is the dominance of the second Rossby mode. The result disagrees with Furnes (1987) who found the gravest mode to be dominant in a study of topographic waves in the Norwegian Trench. However the results are hardly comparable because Furnes (1987) run the model for a different wind field and a steeper bottom topography. Surprising results in modal dominance have also been obtained by Church et al. (1986).

As shown in Fig. 7, the dynamics of the interface ζ_0 is dominated by two mechanisms: The wind induced Ekman pumping and the horizontal divergence due to topographic Rossby waves. The superimposed sub-inertial oscillations are of the same form as the flow pattern of free barotropic Rossby waves where the interface reflects the divergence pattern of these waves. As a conse-

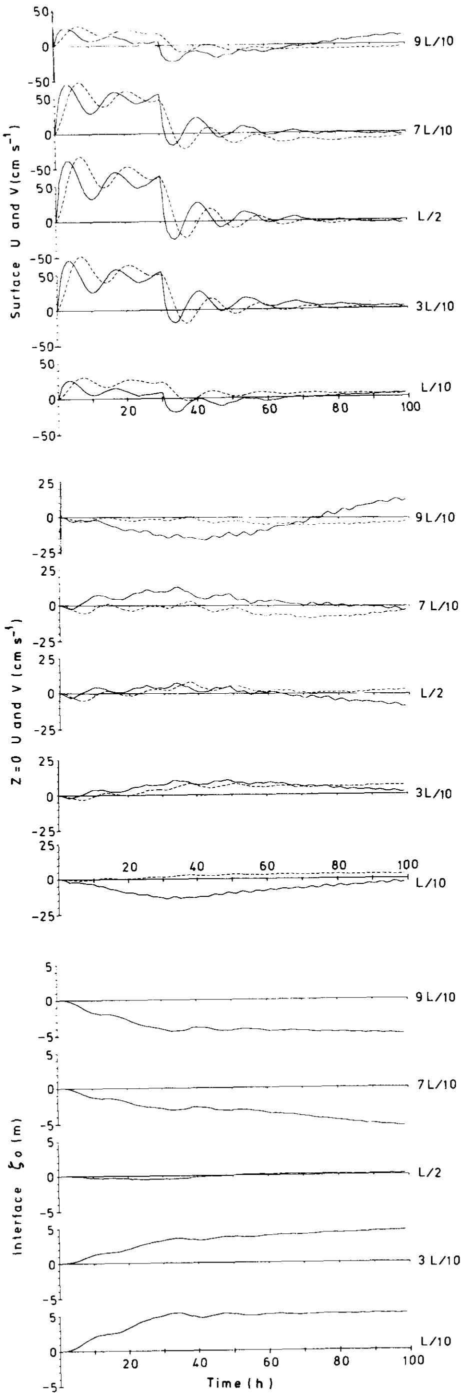

Fig. 5. Time series for the complete model showing the response of u (dashed lines), v (full lines) and ζ_0 at 5 across-channel positions.

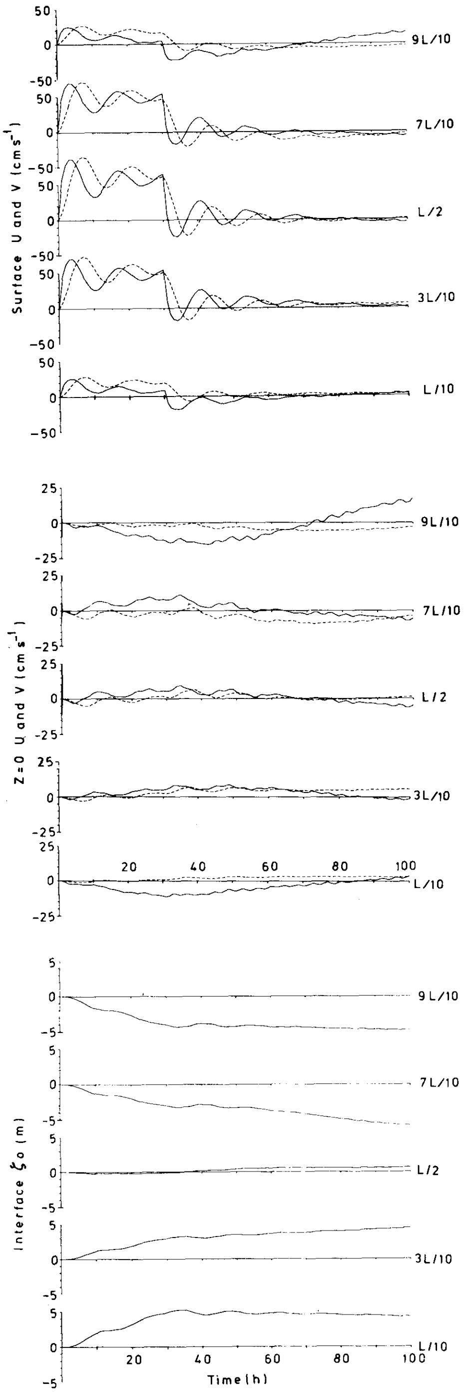

Fig. 6. Time series for a simplified model showing the response of u (dashed lines), v (full lines), and ζ_0 at 5 across-channel positions.

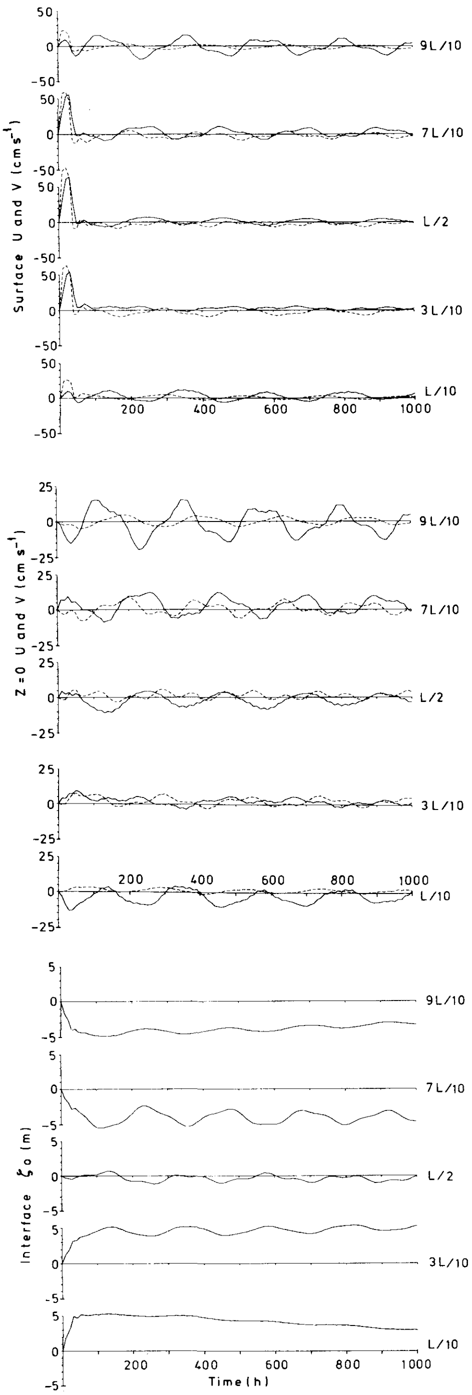

Fig. 7. Time series for 700 km wavelength showing the response of u (dashed lines), v (full lines), and ζ_0 at 5 across-channel positions.

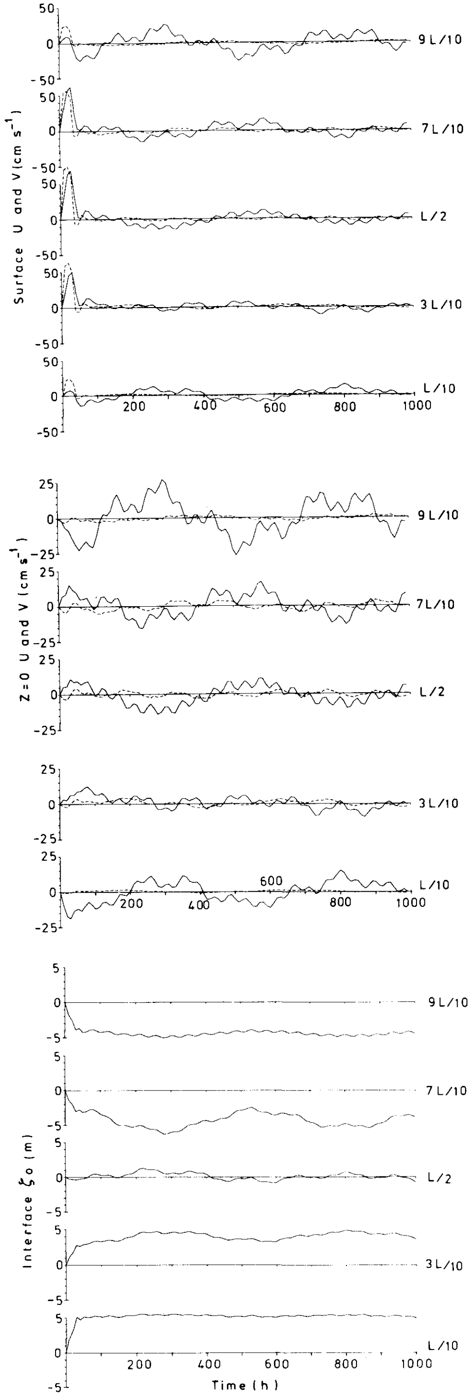

Fig. 8. Time series for 2000 km wavelength showing the response of u (dashed lines), v (full lines), and ζ_0 at 5 across-channel positions.

quence, the interfacial oscillations are dominated by the second Rossby mode. From a physical point of view, Rossby waves give rise to forced vertical motion and the response of the baroclinic field can be compared with responses to external forcing manifested as forced waves on the interface ζ_0.

Model simulations for 2000 km wavelength show a very similar amplitude response as for 700 km wavelength. For the 2000 km wavelength, the pre-dominating response of the second Rossby mode is manifested in an oscillating pattern with

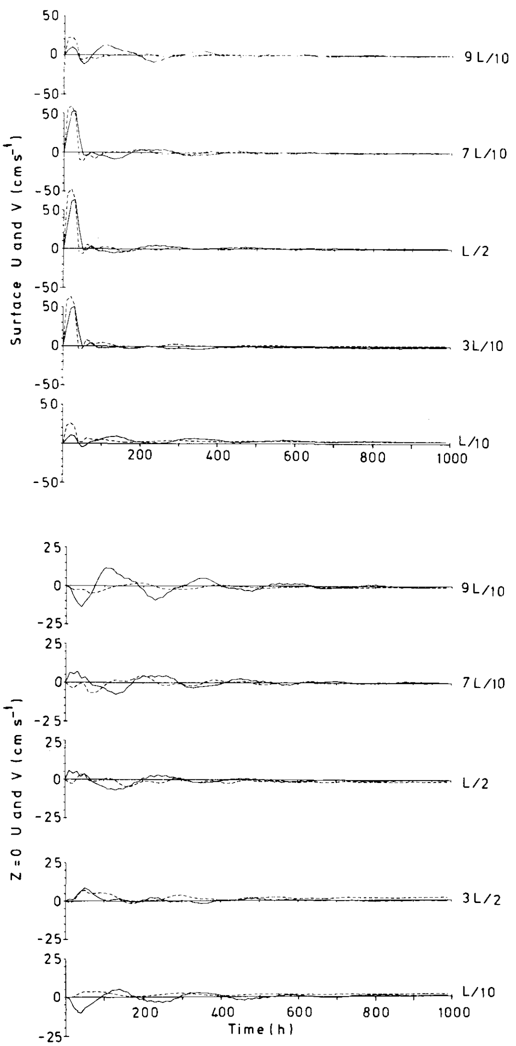

Fig. 9. Time series with an Ekman layer of 5 m showing the response of u (dashed lines) and v (full lines) at 5 across-channel positions.

period 525 h. The gravest mode shows oscillations of about 144 h period.

The simulations for wavelengths of 700 km and 2000 km, indicate a similar response over a spectrum of wavelengths. The reason that there is no accumulation of energy at the ZGS wave length is most likely to be caused by the open channel formulation and application of periodic boundary conditions along the channel. Each free wave will propagate through the area and energy will not be accumulated.

In the real ocean, the wind can be described as wave bands about basic wavelengths and not as particular waves. The ocean will respond over a similar wave band. From this point of view, an accumulation of energy for basic wavelengths about the ZGS seems reasonable. Additionally, ocean boundaries will affect the propagation of free waves and cause accumulation of energy for particular wavelengths.

Fig. 9 shows that the bottom friction affects the current through a decay with time. Most prominent is the damping of the long periodic oscillations. The decay time for these oscillations agrees well with the e-folding parameter in Table 1.

6. Concluding remarks

The main aim in this study has been to present a new method in the study of wind induced motion over varying bottom topography. This two-layer formulation with a stratified upper layer joined continuously to a homogeneous lower layer can be interpreted as splitting a continuous density profile. The formulation makes it feasible to extend standard normal mode separation methods to problems with varying bottom topography.

It is apparent from model simulations that topographic effects are of great importance and the time series show that the flow in the channel is dominated by topographic Rossby waves. Here the dominance of the second Rossby mode should be noted. While the dispersion relationships for the topographic waves are less influenced by stratification, these waves are prominent in generating interfacial displacements.

The main advantage with the eigenmode solution technique has been in the study of the natural oscillations for the channel. The eigensolutions have revealed a simplified coupling pattern between the barotropic and baroclinic part of the motion. This simplified coupling has resulted in modified baroclinic modes for this specific two layer formulation.

7. Acknowledgment

Thanks are due to A. Evjen and L. P. Røed for valuable advice.

REFERENCES

Allen, J. S. 1975. Coastal trapped waves in a stratified ocean. *J. Phys. Oceanogr. 5*, 300–325.

Clarke, S. J. 1977. Observations and numerical evidence for wind-forced coastal trapped long waves. *J. Phys. Oceanogr. 7*, 231–247.

Church, J. A., Freeland, H. J. and Smith, R. L. 1986. Coastal trapped waves on the East Australian Continental Shelf. Part 1: Propagation of modes, *J. Phys. Oceanogr. 16*, 1929–1943.

Fennel, W. 1989. Inertial waves and inertial oscillations in channels. *Continental Shelf Res. 9*, 403–426.

Fjeldstad, J. E. 1964. Internal waves of tidal origin. *Geofysiske Publikasjoner 2*, 25 (5).

Furnes, G. F. and Mork, M. 1987. Formulation of a continuously stratified sea model with three-dimensional representation of the upper layer, *Coastal Engineering 11*, 415–444.

Furnes, G. F. 1987. *On bottom trapped waves over the Western slope of the Norwegian Trench.* Bergen Scientific Centre, Report 6/7, 33 pp.

Gill, A. E. and Clarke, A. J. 1974. Wind-induced upwelling, coastal currents and sea-level changes. *Deep Sea Res. 21*, 325–345.

Gordon, R. L. and Huthnance, J. M. 1987. Storm-driven continental shelf waves over the Scottish continental shelf. *Continental Shelf Research 7*, 1015–1048.

Heaps, N. S. and Jones, J. E. 1985. A three-layered spectral model with application to wind-induced motion in the presence of stratification and a bottom slope. *Continental Shelf Research 4*, 279–319.

Huthnance, J. M., Mysak, L. A. and Wang, D.-P. 1986. Coastal trapped waves. Baroclinic processes on Continental Shelves, *Coastal and Estuarine Science 3*, American Geophysical Union.

Mork, M. 1971. *On the time-dependent motion induced by wind and atmospheric pressure in a continuously stratified ocean of varying depth.* Geophysical Inst. Dep. A, University of Bergen, Norway.

Mork, M. 1972. On ocean response to atmospheric forces. Rapp. P. V. Reun., *Cons. Int. Explor. Mer 162*, 184–190.

Mysak, A. M. 1980. Recent advance in shelf wave dynamics. Rev. Geophys. *Space Phys. 1*, 211–241.

Wang, D.-P. 1975. Coastal trapped waves in a baroclinic ocean, *J. Phys. Oceanogr. 5*, 326–333.

Wang, D.-P. and Mooers, C. N. K. 1976. Coastal trapped waves in a continuously stratified ocean. *J. Phys. Oceanogr. 6*, 853–863.